Zhao, Yang; Liu, Xiao Long; Ma, Sheng Xiang; Wang, Wen Jing; Ning, Xi Jing; Zhao, Li; Zhuang, Jun

Light-optimized photovoltaic self-powered NO_2 gas sensing based on black silicon

Published in:
Sensors and Actuators, B: Chemical

DOI:
10.1016/j.snb.2021.129985

Published: 01/08/2021

Document Version
Peer-reviewed accepted author manuscript, also known as Final accepted manuscript or Post-print

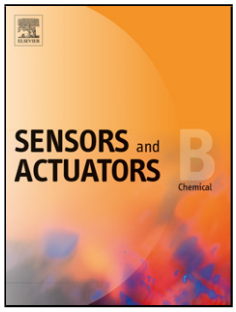

Light-optimized photovoltaic self-powered NO_2 gas sensing based on black silicon

Yang Zhao (Conceptualization) (Methodology) (Investigation) (Visualization) (Writing - original draft), Xiao-Long Liu (Conceptualization) (Writing - review and editing), Sheng-Xiang Ma (Conceptualization) (Investigation), Wen-Jing Wang (Investigation), Xi-Jing Ning (Supervision), Li Zhao (Supervision), Jun Zhuang (Validation) (Writing - review and editing) (Supervision)

PII: S0925-4005(21)00554-2

DOI: https://doi.org/10.1016/j.snb.2021.129985

Reference: SNB 129985

To appear in: *Sensors and Actuators: B. Chemical*

Received Date: 9 December 2020

Revised Date: 8 April 2021

Accepted Date: 13 April 2021

Please cite this article as: Zhao Y, Liu X-Long, Ma S-Xiang, Wang W-Jing, Ning X-Jing, Zhao L, Zhuang J, Light-optimized photovoltaic self-powered NO_2 gas sensing based on black silicon, *Sensors and Actuators: B. Chemical* (2021), doi: https://doi.org/10.1016/j.snb.2021.129985

Light-optimized photovoltaic self-powered NO_2 gas sensing based on black silicon

Yang Zhao,† (email: 18210720016@fudan.edu.cn), Xiao-Long Liu,† (email: liuxl15@fudan.edu.cn), Sheng-Xiang Ma,† (email: 17210720009@fudan.edu.cn), Wen-Jing Wang,† (email: 19110720005@fudan.edu.cn), Xi-Jing Ning,‡ (email: xjning@fudan.edu.cn), Li Zhao,§,* (email: lizhao@fudan.edu.cn), Jun Zhuang†,* (email: junzhuang@fudan.edu.cn)

†Shanghai Ultra-Precision Optical Manufacturing Engineering Center, Department of Optical Science and Engineering, School of Information Science and Technology, Fudan University, Shanghai 200433, China

‡Applied Ion Beam Physics Laboratory, Institute of Modern Physics, Department of Nuclear Science and Technology, Fudan University, Shanghai 200433, China

§Collaborative Innovation Center of Advanced Microstructures, State Key Laboratory of Surface Physics and Department of Physics, Fudan University, Shanghai 200433, China

*Correspondence should be addressed to J.Z. (email: junzhuang@fudan.edu.cn) or L.Z. (email: lizhao@fudan.edu.cn).

Highlights

- Photoelectron-based room-temperature gas sensing using N-hyperdoped silicon.
- Novel photovoltaic self-powered gas sensing under asymmetric light illumination.
- Multidimensional regulation of sensing by light intensity and wavelength.
- Excellent overall sensing performance under optimized light parameters.

ABSTRACT

The NO_2 sensing performance of a special lateral photovoltaic self-powered gas sensor based on the N-hyperdoped microstructured silicon (N-Si) is systematically studied under the different light

illumination. The dependence of sensing characteristics on light intensity and wavelength is obtained, respectively. Results show that the sensing properties can be changed effectively by the different intensities and wavelengths, suggesting that a multidimensional regulation/optimization for the sensing characteristics is possible by light. More interestingly, the light with wavelength of 940 nm and intensity of ~18 $\mu W/cm^2$ could bring a comprehensive optimization for gas sensing, under which the N-Si sensor exhibits the excellent overall performance with simultaneously the low light power needed, good gas response, high sensitivity, wide detectable range and short response time at room temperature.

Keywords: black silicon; gas sensor; self-powered gas sensing; lateral photovoltaic effect; nitrogen dioxide

1. Introduction

Self-powered gas sensing is attracting widespread interests in potential applications like flexible electronics [1], wireless sensor networks for IoTs [2,3], and healthcare devices [4,5]. An active self-powered sensor could harness the ambient energy [6,7] to power the sensing function without the need for external electric power [8]. Under the light illumination, the photovoltaic (PV) self-powered gas sensing could be achieved by photovoltaic effects, which is suitable for in-door or remote air monitoring [7,9–15]. Different strategies towards the PV self-powered gas sensing have been demonstrated [16]. For examples, based on the p-n heterojunction structures [9–15], the sensing signal can be induced under light illumination without external electric power supply. In our recent work, a novel PV self-powered scheme through an asymmetric light illumination was proposed based on the N-hyperdoped microstructured silicon (N-Si) to widen the dynamic range for NO_2 gas sensing [17]. The lateral symmetrical structure of the N-Si device could generate a zero-biased photocurrent as the sensing signal owing to the lateral photovoltaic effect under the asymmetric light illumination [17–20], which is different from other PV self-powered sensors [9–15,21–23] in terms of device structure and working principle. Besides, the material used in the sensor is special, which is the kind of silicon prepared by high-intensity femtosecond-pulsed laser irradiation in specific

ambient atmosphere, and also called black silicon for its enhanced optical absorption [24-28]. Irradiation of femtosecond (fs)-pulsed laser results in microstructured surface and certain element from ambient atmosphere being hyperdoped in silicon, which could bring a series of unique properties. For example, besides the increased surface area, the microstructured surface has rich surface defects [24], in favor of gas absorption compared with the planar one. Different hyperdoped element could also lead to the different gas sensing properties. For instance, S-hyperdoped silicon was found to be sensitive to ammonia gas with the help of light [19], while N-hyperdoped one studied here appears more sensitive for NO_2. Moreover, the microstructures and the hyperdoped impurities could bring unique optoelectronic property, in which more electron-hole pairs are excited. For PV self-powered gas sensor, this means the potential to optimize and improve the sensing capabilities through light.

The PV self-powered sensor could harness the ambient light energy to power the sensing function. In different application situations, the ambient light may come from nature, such as the sunlight, or be generated by artificial light sources. No matter what kind of scene it is used in, as a self-powered sensor or a low-powered sensor, the law of gas sensing performance varying with light is critical for the applications. In a changing natural light, the law can be used to calibrate the output of the sensor to obtain more accurate results. When the sensor works under an artificial light source or adjustable light, the variation of sensing performance with light could help us to purposefully regulate the sensing properties, e.g., the gas response, sensitivity, response time, detectable range and so on, to meet the different requirements of practical applications [19,29–31]. More meaningfully, considering that various parameters of the light can be changed, such as intensity, frequency, and even the illuminated area, a multidimensional regulation or optimization for sensing properties might be achieved by light, and by which it is possible to obtain good comprehensive sensing performance. These potential and attractive characteristics are the motivation for us to study the gas sensing performance as a function of illumination, especially considering the unique optoelectronic property of the material and the special PV self-powered scheme as mentioned above [16-20].

In this work, for the lateral PV self-powered NO_2 gas sensor based on N-Si, the NO_2 sensing

performance is systematically investigated under the different light illumination conditions. Intensity-tunable monochromatic LEDs from visible to infrared ranges are chosen as the light source. Under each wavelength, the dependence of the gas response, sensitivity, response time, and detectable range on the light intensity is studied. The change of these sensing characteristics with wavelength is also given. Then, an overall optimization is considered based on the results. Under an optimal light condition, the excellent comprehensive sensing performance with reduced light power dependence, good gas response, high sensitivity, wide detectable range, and short response time is shown at room temperature. Finally, the mechanism for this is discussed.

2. Materials and method

The N-hyperdoped silicon was prepared on n-type monocrystalline Si (100) wafer with high resistivity (3–5 kΩ·cm) and thickness of 250 μm. The silicon surface was irradiated by femtosecond laser pulses (1 kHz, 190 fs, 515 nm) under a NF_3 atmosphere (70 kPa). The fluence of the focused beam was about 6.4 kJ/m^2 and a microstructured area of 3 × 8 mm^2 was produced by the laser scanning. The surface morphologies of the laser ablated area can be observed by the scanning electron microscopy (SEM), as shown in Fig. 1a. The aluminum electrodes were thermally evaporated onto the structured region in two coplanar squares with a side length of 2.5 mm and 2.5 mm apart. The schematic diagram of the sensor is shown in Fig. 1b. A more detailed experimental process can be found elsewhere [17].

Before gas sensing measurement, to clarify the self-powered output signal of N-Si sensor, the position-sensitive photocurrent was measured. The incident light was generated from a bromine tungsten lamp (LSH-T150) and then focused to a squared spot size of 0.5 mm in length on the device surface by a focal lens. The device was translated at a step of 0.5 mm and at the same time the output photocurrent was recorded at different positions.

After fabricated and nature aging for about 3 days, the sensor is used for the measurements. For self-powered gas sensing, the sensor was placed under an asymmetric light illumination setup [17] and the output photocurrent was used as the sensing signal. One of the monochromatic LEDs with

different central wavelengths (λ = 455, 730, and 940 nm) was applied as the light source to illuminate a half of the surface of the N-Si gas sensor. The light intensity was characterized by the power density (P), defined as the light power received per unit area. The light intensity received by N-Si surface was changed by applying different bias voltages to the LED and estimated by a commercial Si photodetector in the same position. Under the asymmetric light illumination, gas sensing measurement was performed by using a homemade static volumetric system and the concentration is calculated by the volume ratio of the standard gas to that of the testing chamber. The NO_2 gas in the experiment was calibration gas (≥99.9%) purchased from Air Liquide Shanghai Co., Ltd. The external bias source for LEDs was provided and the output current signal was measured simultaneously by using a (Keysight B2902A) source-and-measurement unit. All the measurements were taken at room temperature (24 ± 0.5 °C). The relative humidity of the indoor air was controlled at about 32% during the measurement. The ambient temperature and the relative humidity (RH) were recorded by using a digital hygrothermograph mounted inside the chamber.

For studying the effect of the relative humidity (RH) on the NO_2 response properties, the chamber was first filled with indoor air, and the humidity in the chamber was changed with a humidifier (Baseus). The response to RH was reflected in the stabilized readout photocurrent. Then, a specific concentration of NO_2 was injected into the chamber by a gas syringe, before the chamber was opened to re-expose the sensor to indoor air. These procedures were repeated at different RH readouts.

The relative gas response R was defined as $R = (I_g - I_a)/|I_a| = \Delta I/|I_a|$, where I_g was the output photocurrent in target gas and I_a represented the current in air (or the baseline current). The sensitivity S was referred to the change rate of photocurrent with gas concentration, obtained from the slope of the calibration curve (current versus gas concentration plot). Response time (t_{res}) was defined as the time taken from baseline (I_a) to 90% of the maximum amplitude of the response ($90\% \cdot \Delta I$) within the measurement time, whereas recovery time (t_{rec}) was the time to recover from final value (I_g) to 10% response amplitude ($10\% \cdot \Delta I$).

For understanding the influence of light on gas sensing properties, the external quantum

efficiency (EQE) of the device was given, which was calculated from the spectral responsivity ($R_s(\lambda)$) and defined as $\mathrm{EQE} = 1.24R_s/\lambda$. The R_s was measured using the light from the bromine tungsten lamp (LSH-T150) which was filtered through a monochromator (Omni-λ300). The monochromator scanned in steps of 100 nm from 500 to 1100 nm and a commercial Si photodetector was used for calibration.

3. Results and Discussion

3.1. Photocurrent under the asymmetrical light illumination

Fig. 1b and 1c are the surface and the section schematic diagrams of N-Si gas sensor. First off, the lateral photovoltaic effect (LPE) of N-Si is measured. As shown in Fig. 1b, as the focused light spot (0.5 mm in length) scans along the brown line, the photocurrent change between the electrodes is recorded without a bias voltage supply. Fig. 1d shows the dependence of the measured photocurrent on the position of the light spot, the x value represents the distance between the incident light spot in reference to the midpoint of the scanning route (symmetric center of the device surface). It can be seen that the photocurrent is induced when $x \neq 0$, and this photocurrent changes from one polarity to the other as the light spot moves across the midpoint of the scanning route ($x = 0$). The phenomenon is known as the lateral photovoltaic effect (LPE) and is observed on similar device structures [32–34]. However, when $x = 0$, the sensor is illuminated with a laterally symmetric light, and there is no photocurrent output. For N-Si gas sensing, we attempt to utilize the photocurrent produced by LPE to detect the target gas adsorbed on the surface, and to make a full use of the surface area as well as get a maximum photocurrent, a half of the surface is illuminated by the light source whereas the other half is kept dark; the method is called the asymmetric light illumination (ALI), and the method is shown in Fig. 1c.

Under the ALI with the light source of a LED, the current-voltage (I-V) characteristic of the sensor is measured and compared with that in the dark, as shown in Fig. 1e. The linear curve in dark indicates a fine Ohmic contact between the Al film and the sensing surface. Under the ALI, a negative photocurrent is obviously produced at zero bias voltage. As shown in Fig. 1c, when a half of the N-Si

surface is illuminated without bias voltage, a number of electron−hole pairs are generated and tend to diffuse to the other half. The electrons diffusion contributes to a negative current (I^-) and the holes diffusion contributes to a positive one (I^+). The number of the photogenerated electrons (n_{pe}) and holes (n_{ph}) are equal, but the mobility of electrons (μ_e) in N-Si is higher than holes (μ_h), resulting in a larger generated electron current than that of hole ($|I^-| > |I^+|$) under the nature of current $I \propto \mu n$. Thus, the total current $I^- + I^+ < 0$ leads to the measured negative zero-biased photocurrent under ALI. Previously, we find this photocurrent changes monotonously with the concentration of the analyte gas [17], which means that the sensor can work without a bias voltage, referring to the so-called self-powered sensing. In the following, sensing performance in such mode is considered, in which the photocurrent is used as the gas sensing signal.

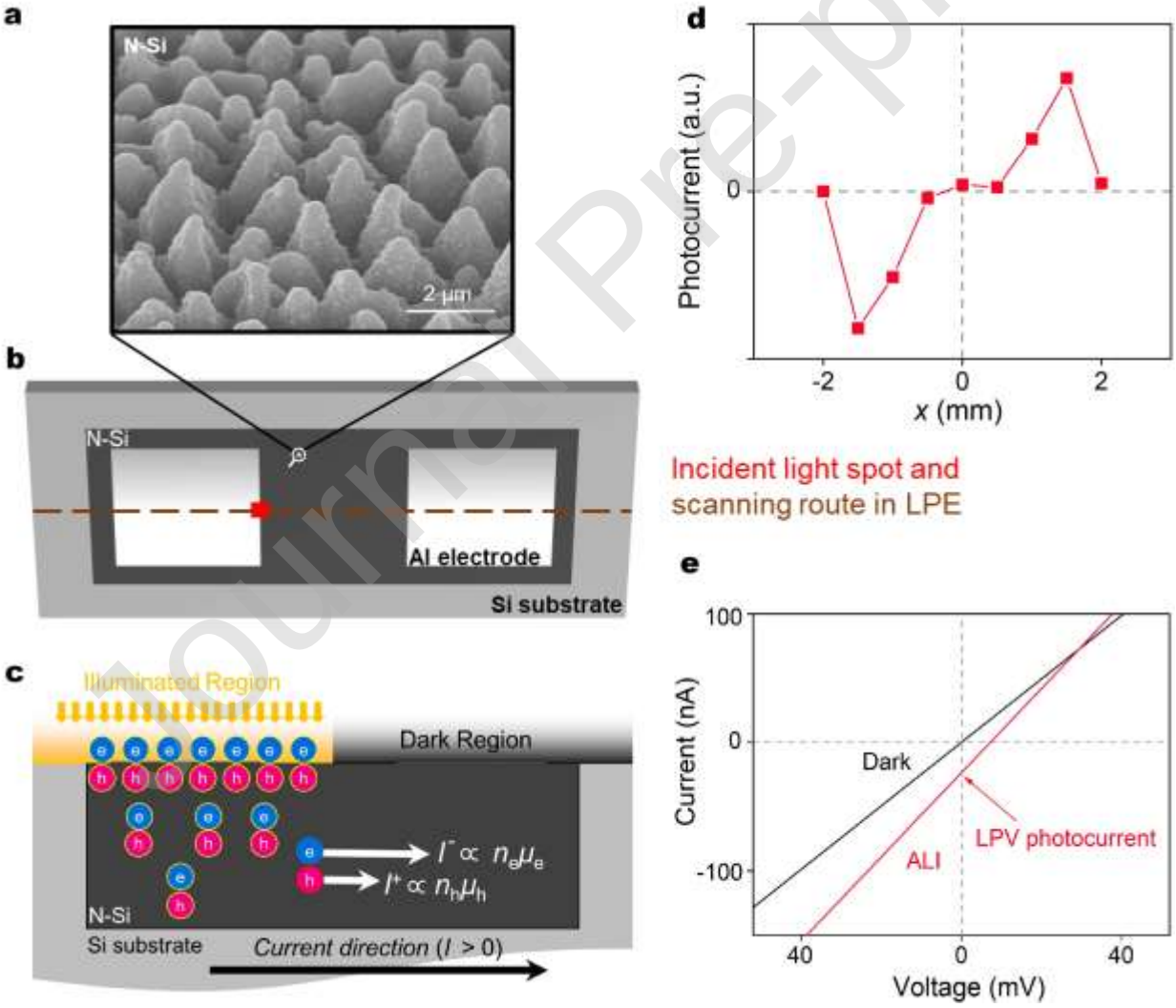

Fig. 1. (**a**) Scanning electron microscopy (SEM) image of the N-Si surface microstructures. (**b**) Schematic diagram of the surface of N-Si gas sensor. The red square dot and the brown dotted line represent the incident light spot and the scanning route in LPE measurement. (**c**) Schematic diagram of the section of N-Si gas sensor under the asymmetric light illumination. The blue and pink circles with yellow edge are the photogenerated electron–hole pairs. (**d**) The zero-biased photocurrent changes with the incident light position between the lateral contacts. x is the distance between the incident light spot and the midpoint of the scanning route. (**e**) Comparison of I-V characteristics of the sensor in the dark and under the asymmetric light illumination.

3.2. Effects of light intensity on sensing properties

Since the photocurrent is used as the signal for detecting the analyte gas, it is naturally expected that its sensing properties could be dependent on the illuminated light intensity. We firstly investigate the effects of the light intensity on the NO_2 response characteristics under the ALI. Here, a red LED (730 nm) is used as the light source, of which the power density (P) can be tuned from 0 to ~2.72 mW/cm^2. In air, the I-V characteristics of the sensor are measured first under the ALI of different light intensities. As shown in Fig. 2a, the magnitude of the photocurrent in air ($|I_a|$) increases with the light intensity. Then, the same procedure is repeated in different concentrations of NO_2 gas from 10 to 2000 ppm. For example, Fig. 2b presents the I-V characteristics of the sensor under the ALI with different light intensities in 100 ppm NO_2. Compared to the baseline photocurrent in air ($I_a < 0$), the photocurrent after the NO_2 adsorption turns into a positive one. This is attributed to that the adsorbed NO_2 induces an increased surface barrier height for photoelectrons [17], leading to the decrease of $|I^-|$ and then resulting in the output photocurrent $I^- + I^+ > 0$. In addition, as shown in Fig. 2b, the photocurrent (I_g) increases dramatically with the light intensity. To intuitively show the dependence of the photocurrent on the light intensity in different NO_2 concentrations, we collect all the photocurrents in the above experiments and plot them in Fig. 2c. Notably, the photocurrent increases from –6.9 nA in air to remarkable ~9 μA in 2000 ppm under P = 2.7 mW/cm^2.

The data in Fig. 2c can be used to calculate the gas response ($R = (I_g - I_a)/|I_a|$) in different NO_2 concentrations and the results are shown in Fig. 2d. Unexpectedly, the gas response (R) is not positively correlated to the light intensity. It first increases and then decreases with increasing light intensity, showing an inverse U-shaped trend at any concentration. Noting the different effects of I_g and I_a on the response ($R = (I_g - I_a)/|I_a|$), this non-monotonicity indicates the different increasing trend of photocurrent in NO_2 (I_g) and in air (I_a) with light intensity increasing. Thus, there is an optimal light intensity value to obtain the highest gas response, indicating that the gas response can be optimized by tuning the intensity of the ALI. As shown in Fig. 2d, the maximum response can be obtained when the light intensity is about P = 0.39 mW/cm^2, i.e., the response is 13200% in 50 ppm and even reaches 38000% in 2000 ppm. This optimal P is located at a lower level within the intensity range of our experiment, meaning the maximum response can be obtained with relatively low light intensity requirement.

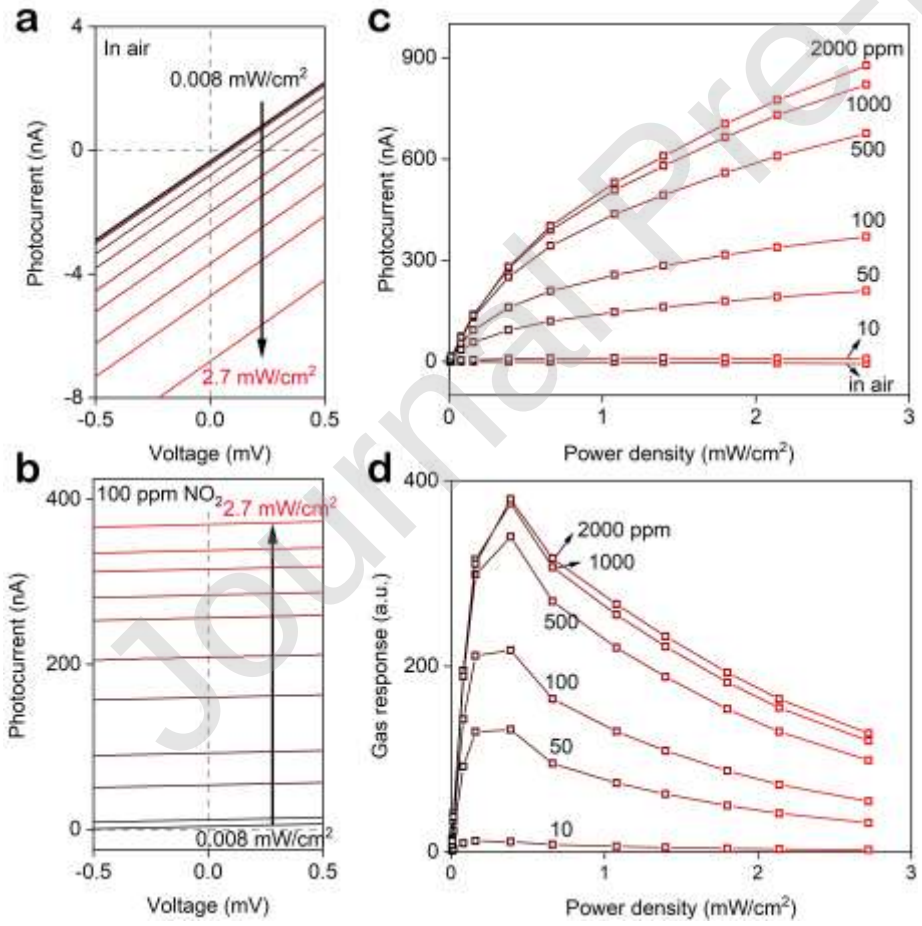

Fig. 2. (**a** – **b**) I-V characteristics of the sensor under different light intensities (quantified by power densities) (**a**) in air, (**b**) in 100 ppm NO_2. (**c**) Photocurrent varies with power densities in air and different NO_2 concentrations. (**d**) Gas response ($\Delta I/|I_a|$) to different NO_2 concentrations varies with power densities. The central wavelength of the light is 730 nm.

To verify the trend of the response R and also get the response speed, the transient photocurrent response to 50 ppm and 100 ppm NO_2 are measured with varied power densities (P), as shown in Fig. 3a. In order to observe the response repeatability of the sensor, the repeated response to 50 ppm NO_2 is also measured and shown in Fig. 3b. It can be seen that the response reproducibility of N-Si sensor is good. Based on Fig. 3a, the gas response (R) at different power densities is calculated and shown in Fig. 3c, where both curves present inverse U-shaped trend, gaining the maximum response at the same turning point of around P = 0.22 mW/cm^2. Compared with the results in Fig. 2d, the power density required at the turning point is slightly different because of the two different measurement methods. Despite this, the similar trends verify the non-monotonic dependence of the gas response on the light intensity. As to the response time shown in Fig. 3d, the curves show the opposite trend to the gas response ones and the shortest response time is obtained also at the light intensity of ~0.22 mW/cm^2. That is, at the same certain density which is referred to as the optimal intensity in the following, the gas response reaches the highest while the response time is the shortest. For the recovery time, it seems to be insensitive to the change of light, the value of which for 50 ppm is ~10 s.

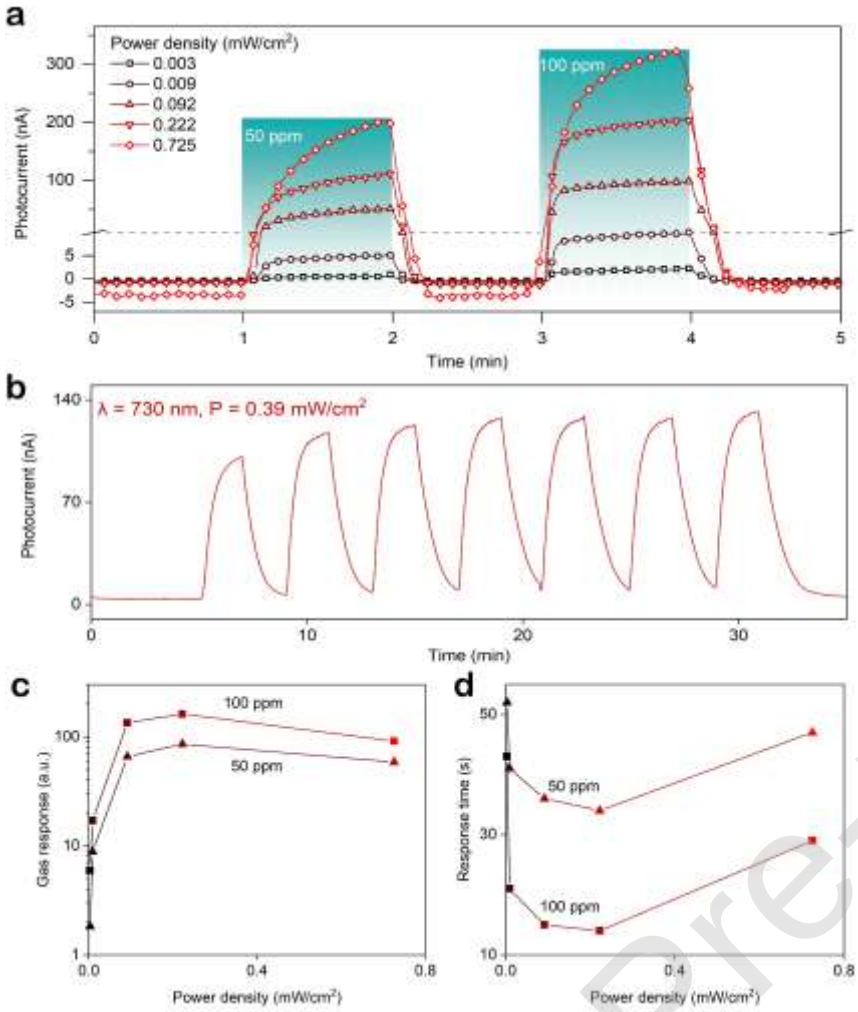

Fig. 3. (**a**) Photocurrent transients in response to 50 ppm and 100 ppm NO_2 under different power densities. (**b**) Repeated response to 50 ppm NO_2 under power density of 0.39 mW/cm^2. (**c**) Gas response ($\Delta I/|I_a|$) and (**d**) Response time varies with power densities, data obtained from (a). The central wavelength is 730 nm.

Sensitivity (S) is another key parameter in gas sensing which is obtained by the following method. Using the data in Fig. 2c, we plot the dependence of photocurrent (I) with the concentration ($[C]$) at different illumination levels in Fig. 4a. The I-$[C]$ calibration curves are fitted by using an extended Langmuir adsorption isotherm equation (LangmuirEXT1) [17], i.e., $I = (a_2 b_2 [C]^{1-c_2})/(1 + b_2 [C]^{1-c_2})$, and all coefficients of determination of the fitted curves exceed 0.9. According to the definition, the sensitivity (S) is then calculated from the first-order derivative of the calibration curves. As seen in Fig. 4b, at any concentration, the sensitivity increases monotonously with the light intensity. Different from

the gas response (R) which is defined by the relative change to the baseline, the sensitivity here is defined by the absolute value of the change in signal, independent of the baseline. By definition, it represents the concentration resolution capability. At certain light intensity in Fig. 4b, the sensitivity curve also indicates the dynamic range of concentration when a lowest detectable signal is defined. Therefore, the curves in Fig. 4b show that the dynamic range of concentration or the detectable range is broadened with the increment of light intensity. Particularly for high concentration, the increased sensitivity means the increment of the upper limit of detection. To intuitively verify this conclusion, we measured the photocurrent transients in response to 5–2000 ppm NO_2 under power densities (P) from 0.002 mW/cm^2 to 0.844 mW/cm^2, as shown in Figs. 4c–4f. At a very weak light intensity of P = 0.002 mW/cm^2, the photocurrent gradually shows the sign of saturation from 500 ppm NO_2 (Fig. 4c). After the P is increased to 0.077 mW/cm^2, the sensor can respond properly to 1000 ppm NO_2 and start to saturate from 2000 ppm (Fig. 4d). Furthermore, there is no sign of saturation in 2000 ppm when the P is increased to 0.186 mW/cm^2 and above (Figs. 4e and 4f).

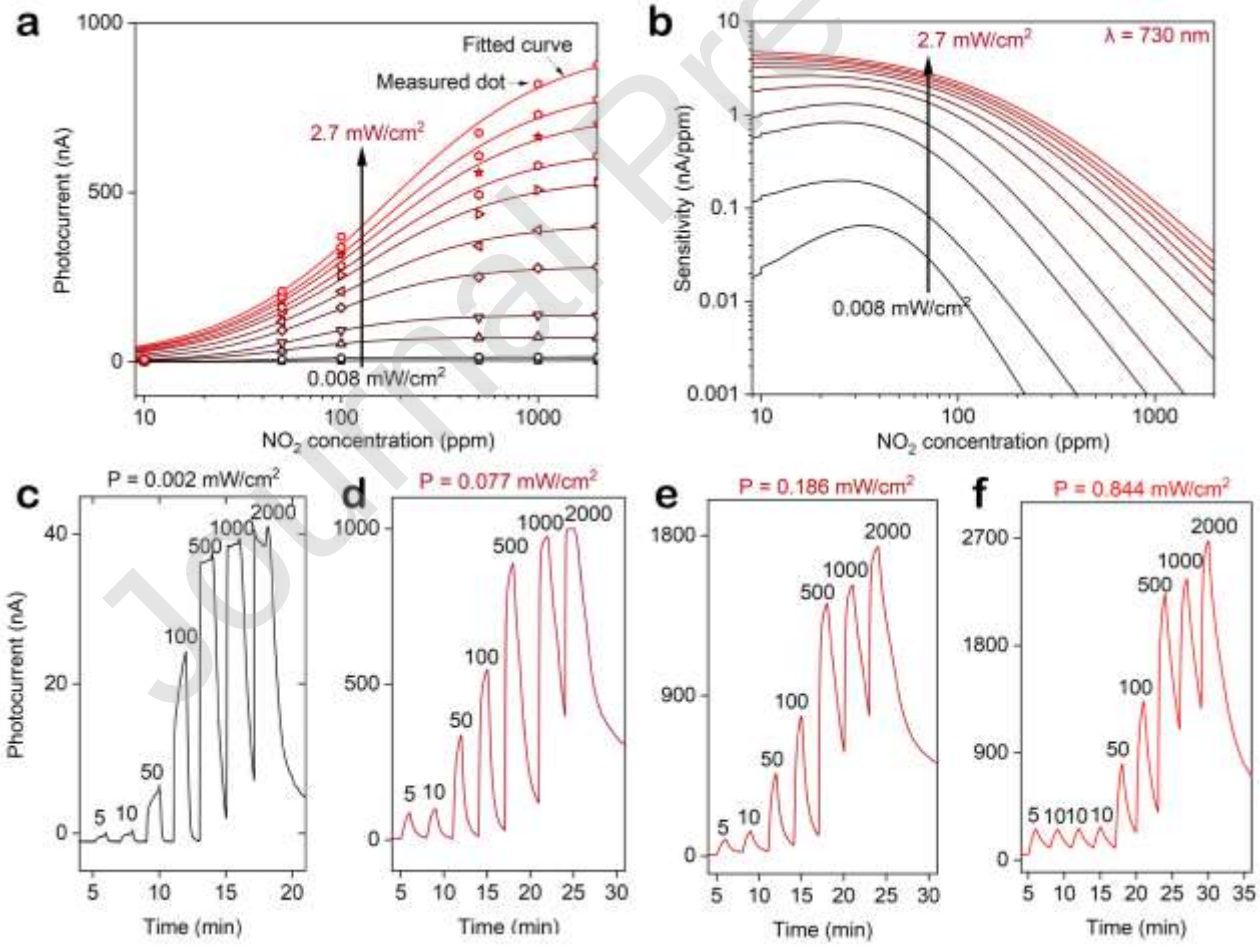

Fig. 4. (**a**) Photocurrent varies with NO_2 concentration (dots, obtained from Fig. 2c) and corresponding calibration curves (lines, fitted by function LangmuirEXT1) under different power densities. (**b**) Gas sensitivity varies with NO_2 concentration (calculated from the first-order derivatives of the calibration curves) under different light densities. (**c** – **f**) Photocurrent transients in response to 5–2000 ppm NO_2 under different power densities: (**c**) P = 0.002 mW/cm^2, (**d**) P = 0.077 mW/cm^2, (**e**) P = 0.186 mW/cm^2, and (**f**) P = 0.844 mW/cm^2. The central wavelength is 730 nm.

Interestingly, for low concentration, the detectable limit also tends to expand with increasing light intensity, reflected in the enhanced sensitivity and transient response to ~5 ppm NO_2 in Fig. 4b and Figs. 4c–4e, respectively. To observe more clearly the improved low concentration detection capability of the sensor, the transient photocurrent response to ppb-level NO_2 concentrations are measured under illumination of a white LED with operating power of ~45 mW (much higher than those of monochrome LEDs), as displayed in Fig. S1. Evidently, the sensor can detect low NO_2 concentration to ppb level if the light power is enough. These results indicate that the upper and lower limits of detection are expanded due to the improvement of sensitivity caused by the increment of illuminated light intensity. That is, increasing the light intensity is beneficial for improving both the concentration resolution capability and detectable range.

3.3. Effects of light wavelength on sensing performance

The hyperdoped silicon exhibits broadband optical absorption and spectral response from UV (ultraviolet) to NIR (near-infrared) range [24-28], so changing the light wavelength could provide another effective way to regulate or optimize the sensing performance. In the following, besides the red (730 nm) light used in the above, the sensing performance of our device is also investigated under blue (455 nm) and NIR (940 nm) light, respectively. The experiments for measuring the gas response, response time, and sensitivity etc. as in Figs. 2–4 are repeated with different light wavelengths. As shown in Fig. S2 and Fig. S3, the variation trends of sensing characteristics on light intensity are similar as described above. Specifically, the gas response at 455 nm (Fig. S2a) and 940 nm (Fig. S3a) present the same inverse U-shaped trend with the change of light intensity compared to Fig. 2d.

However, the peak gas response is different and located at different intensity of ~0.38, 0.39, and 0.10 mW/cm^2, with the wavelength of 455, 730, and 940 nm, respectively, meaning that the gas sensing performance is also related closely to light wavelength.

To intuitively show the dependence of sensing behavior on light condition, the changes of gas response to 50 ppm NO_2 with light intensity at different wavelengths are extracted as Fig. 5a. Apparently, the value varies with either light intensity or light wavelength. Moreover, to further observe the effect of light wavelength and intensity on sensing performance, other comparisons are also made at NO_2 concentration of 50 ppm. Fig. 5b and Fig. 5c present the curves of sensitivity and response time varies with light intensity at the three wavelengths, respectively. The results show that the sensing properties are determined by both the light intensity and wavelength, indicating the multidimensional regulation for gas sensing characteristics can be obtained by light. In other words, light offers more possibilities to optimize the sensing properties. For instance, as mentioned above, at 730 nm wavelength the gas response can reach 13200% in maximum for 50 ppm NO_2 by varying light intensity, whereas with the change of light wavelength, the value can be further increased to 37500% at the optimal intensity of 455 nm, as shown in Fig. 5a. Therefore, for N-Si sensor, changing the parameters of ALI makes the multidimensional regulation for sensing performance possible, by which a certain sensing characteristic can be optimized maximally to meet the different requirements in practical application.

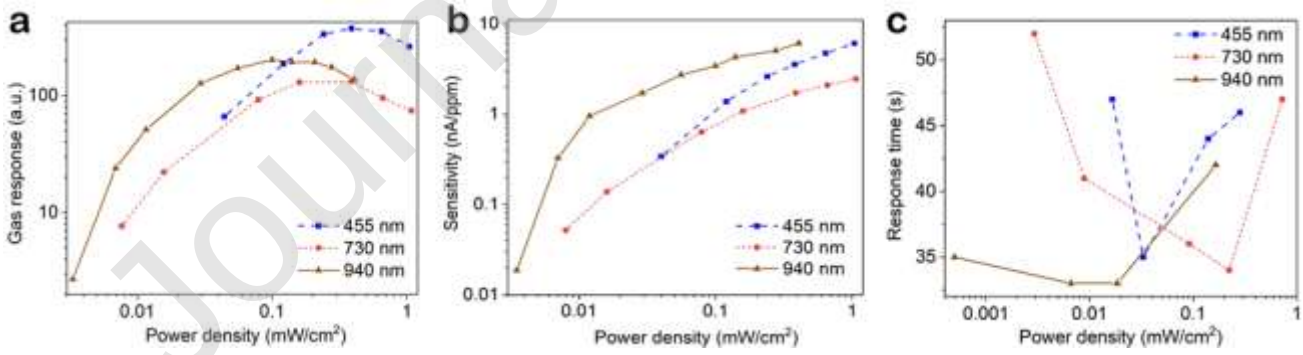

Fig. 5. Comparison of the changes of (**a**) gas response, (**b**) gas sensitivity and (**c**) response time with power densities at the three wavelengths. The NO_2 concentration is 50 ppm.

Then, the interesting question is based on the multidimensional regulation capability of light, whether we can obtain the overall optimization for gas sensing characteristics by choosing a proper

illumination light intensity and wavelength. Considering the ambient light may be weak in some cases, light intensity or the light energy needed is also included as an index in the overall sensing performance. From the gas response curves at different light wavelengths, as shown in Fig. 5a, it is obvious that the gas response first appears at low light intensity at 940 nm. In other words, illumination of 940 nm could first excite the gas response. Besides, among the three wavelengths, the light energy required for the peak gas response at 940 nm is the lowest (~0.10 mW/cm^2), and at this light energy, the response value at 940 nm is also higher than those at the other two wavelengths, as exhibited in Fig. 5a. For the commonly used transient response measurement in practical application, the variations of gas response with power density at three wavelengths (730 nm in Fig. 3c, 455 nm in Fig. S2e and 940 nm in Fig. S3e) are similar to that displayed in Fig. 5a. But owing to the difference of the measuring methods as mentioned above, the corresponding power densities at the turning point are slightly different. The value at 940 nm is ~0.018 mW/cm^2, still lower than that ~0.032 mW/cm^2 at 455 nm and ~0.222 mW/cm^2 at 730 nm. More intriguing, as compared in Fig. 5b and Fig. 5c, it is clear that at the ultra-low light intensity of ~0.018 mW/cm^2, under illumination of 940 nm, the sensor shows the highest gas sensitivity (also the widest detectable range, see Fig. 4b) as well as the shortest response time. These results demonstrate that for the overall optimization, the light of 940 nm with intensity of ~0.018 mW/cm^2 is a good choice among the illumination conditions studied here, at which the sensor shows excellent comprehensive sensing performance with low light power needed, good gas response, short response time, and high sensitivity as the comparison in Table 1. Therefore, benefiting from the multidimensional regulation ability of light, we can not only optimize a specific single sensing parameter to its extreme, but also can regulate the overall sensing performance purposefully to keep various sensing characteristics at a higher level.

Table 1 Comparison of comprehensive sensing parameters at different wavelengths.

Wavelength	Sensing parameters to 50 ppm NO_2			
	P (μW/cm^2)	R	t_{res} (s)	S (nA/ppm)
455 nm	18	~8350%	~45.5	<0.34
730 nm	18	~1460%	~40.5	~0.14

940 nm	18	12820%	33	1.31

*The values at 455 nm and 730 nm are estimated from the Fig. S2e, Fig. 3c and Fig. 5.

3.4. Other sensing characteristics and the mechanism of light-optimized sensing

In general, the sensing performance of a gas sensor would degrade with storage time which mainly results from a continuous oxidization in air. To see the long-term reliability of the sensor, the photocurrent transients in response to 50 ppm NO_2 at different light intensities with wavelength of 730 nm were measured for sample fabricated after 3 days and 30 days, as shown in Fig. 6a and 6b, and for clearly, the baseline and the response photocurrent of which are extracted in Fig. 6c. The baseline photocurrent ($|I_a|$) and the response photocurrent (I_g) of the aged sample are decreased to that of the fresh sample. Fig. 6d shows the comparison of gas response ($\Delta I/|I_a|$) and response time vary with power densities after 3-day and 30-day fabrication. Generally, it can be seen that though the gas response is slightly reduced and the response time is prolonged, the light intensity regulated gas sensing property is still practicable. As shown in Fig. 6d, the tendency of response time curve is contrary to that of gas response, showing that the highest gas response and the shortest response time appear at the same power density in the two cases. For the highest gas response, the value is reduced from ~8985% for the fresh state to ~5160% for the aged state, and the corresponding response time is prolonged from ~123 s to ~279 s.

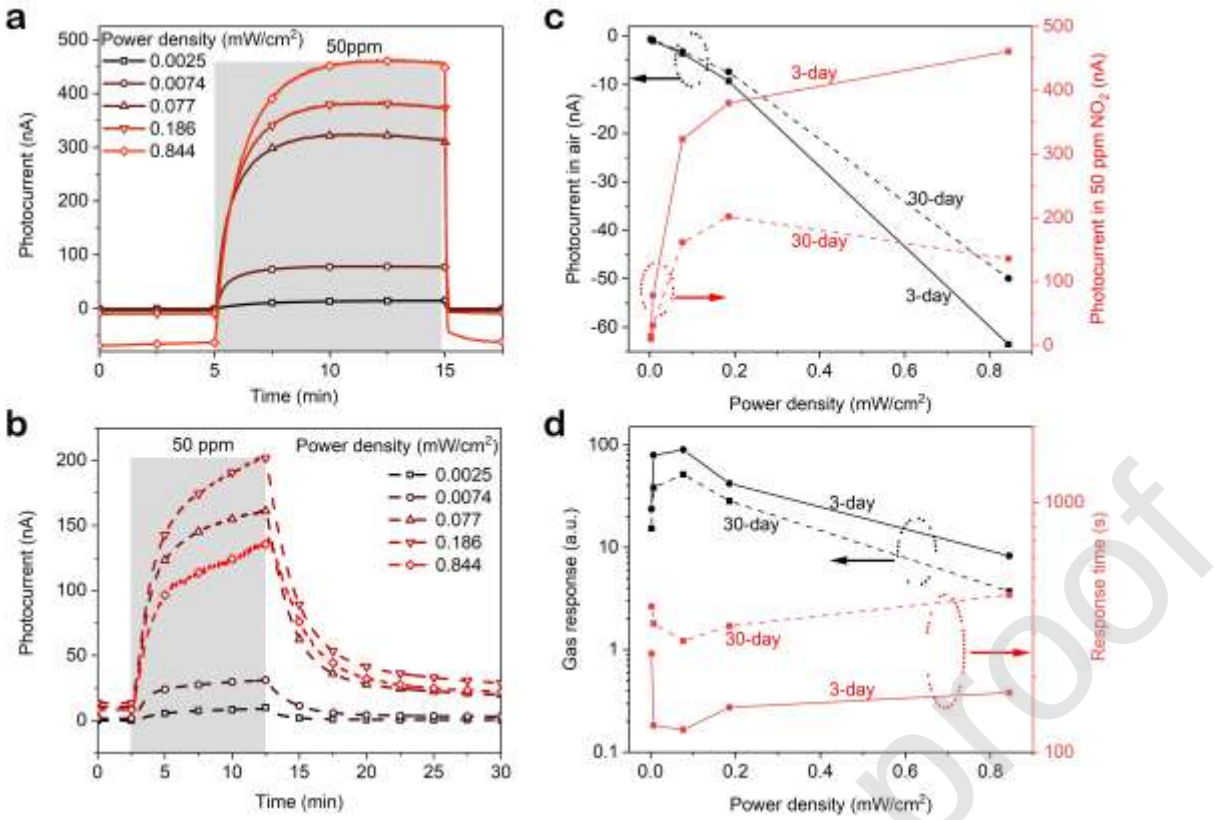

Fig. 6. Gas sensing properties for the sensor after 3-day and 30-day natural aging. (**a** – **b**) Photocurrent transients in response to 50 ppm NO_2 (the sensor exposed to the analyte gas for 10 minutes) under different light intensities (**a**) after 3-day fabrication, (**b**) after 30-day fabrication. (**c**) Comparison of baseline (I_a) and response photocurrent (I_g) in 50 ppm NO_2 vary with power densities after 3-day and 30-day natural aging, data obtained from (a) and (b). (**d**) Comparison of gas response ($\Delta I/|I_a|$) and response time vary with power densities after 3-day and 30-day natural aging, data obtained from (a) and (b). The central wavelength is 730 nm.

Furthermore, we also measured the gas sensing response to other gases commonly used in laboratory environments. The results are displayed in Fig. 7, which shows that the sensor is very selective to NO_2 with significant higher response than NH_3 and other VOC gases (ethanol, isopropanol and acetone). In addition, the effect of the relative humidity (RH) on the 50 ppm NO_2 response under 940 nm with light intensity of ~0.018 mW/cm^2 is also studied. The details can be found in Supplementary Material (Fig. S4). In brief, the gas response ($\Delta I/|I_a|$) is estimated to be 12944%–

535% for RH from 35% to 55% and then drops sharply in the RH above 65%. In 85% RH, the response value is reduced to less than 100%.

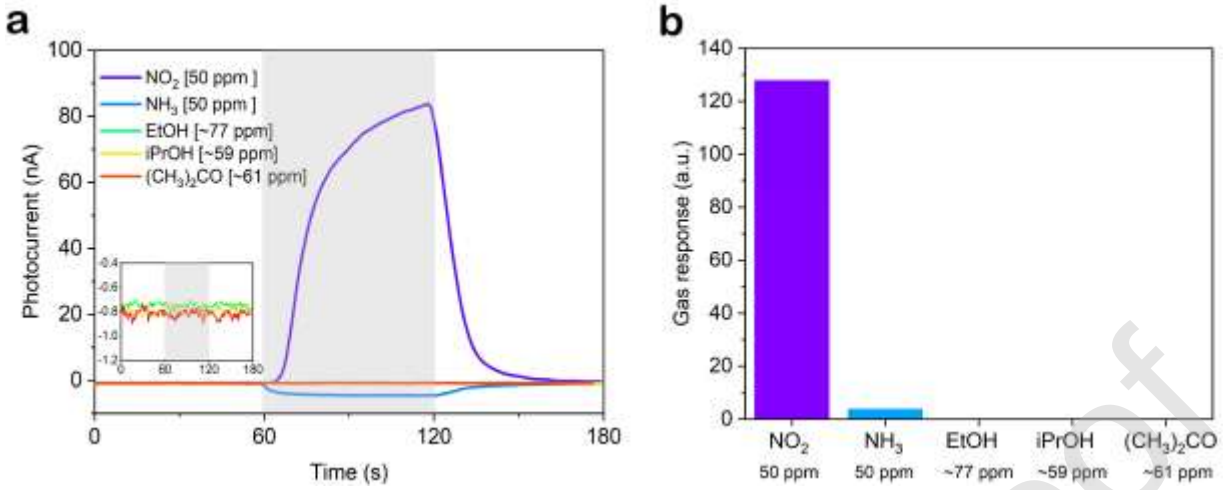

Fig. 7. (**a**) Transient photocurrent in different gas species. (**b**) Gas response ($\Delta I/|I_a|$) to different gas species. The nitrogen dioxides (NO_2) and ammonia (NH_3) used in this experiment are pure standard gases. The volatile organic compounds (VOCs) gases (ethanol, isopropanol, and acetone) are generated by evaporating their liquid phases (a volume of 10 μL for each liquid form). The illumination condition is λ = 940 nm, P = 0.018 mW/cm^2.

Finally, we would like to discuss the mechanism of the light regulated and the NIR (940 nm)-light-enhanced gas sensing. As shown in Fig. 1c and 1e, when a half of the N-Si surface is illuminated without bias voltage, a small negative photocurrent (I_a) can be obtained as the baseline in air (as exampled in Fig. 2c). As discussed above, this output photocurrent based on LPE is caused by the sum of the electron current (I^-) and hole current (I^+). In air, the value of $|I^-|$ is larger than $|I^+|$, resulting in the negative photocurrent output. After the introduction of analyte gas, an increased barrier height is induced on the surface as the adsorbed NO_2 extracted the electrons from the surface [17]. This will hinder the transport of electrons but is beneficial for holes transfer, expressed as the $|I^-|$ decrease and the $|I^+|$ increase. As a result, the output photocurrent (I_g) in NO_2 gas gradually changes to a positive one (as displayed in Fig. 2c) with the increase of gas concentration. The response to the analyte gas is finally reflected in the variation of the output photocurrent, i.e., $I_g - I_a$. Thus, the generated photoelectrons are the main determinant, and the number of which is reflected in I_a. Under

a weak light intensity, a small number of photoelectrons are generated and few of them are obstructed by NO_2 adsorption, expressed as a small photocurrent difference. As light intensity increasing, the number of photogenerated electrons (I_a) increases, and more of them are obstructed in case of the same NO_2 concentration, resulting in the increase of photocurrent difference $I_g - I_a$. Certainly, these two increasing trends could be different. Combined with the definition of gas response ($R = (I_g - I_a)/|I_a|$), the different trends mean the existence of the optimal light intensity or the optimal photoelectron number to obtain the highest gas response as shown in our experiments, e.g., Fig. 2d. On the other hand, at the different wavelengths, the quantum efficiency of the material are generally different, which means the wavelength can also affect the number of photoelectrons. Fig. 8 shows the external quantum efficiency (EQE) spectrum of N-Si in air. The EQE that varies with wavelength indicates that the number of excited photoelectrons in the material is different at different wavelengths. Therefore, the mechanism of wavelength effect on the response is essentially the same as that of intensity, i.e., their effects are realized by affecting the number of the excited photoelectrons. This means we can obtain the optimal photoelectron number for the gas response either by light intensity or wavelength.

Based on the mechanism, we can understand the result of gas response varies with light intensity and wavelength as shown in Fig. 5a. Specifically, at a weak light intensity, if the wavelength 455 or 730 nm with low quantum efficiency is used, it is then possible that the light cannot excite the enough photoelectrons to obtain the optimal photoelectron number and the highest gas response. See Fig. 5a, the weak light intensity ~0.10 mW/cm^2 at 455 or 730 nm is just such case. However, if the wavelength 940nm is used, whose quantum efficiency of N-Si is the highest among the three wavelengths as shown in Fig. 8, even weak intensity ~0.10 mW/cm^2 could still excite enough photoelectrons to obtain the highest gas response, as shown in Fig. 5a.

In contrast, at a relatively strong light intensity, e.g., ~0.38 mW/cm^2, if the illumination wavelength is still 940 nm, the number of excited photoelectrons will exceed its optimal value, resulting in the reduction of gas response, as evident from Fig. 5a. To avoid this, an effective solution is applying the light wavelength with low quantum efficiency, in accordance with which, the optimal photoelectron

number and the highest gas response can be obtained at 455 nm wavelength with lower quantum efficiency, as illustrated in Fig. 5a. Therefore, in order to obtain the optimal photoelectron number and the highest gas response, the light wavelength and intensity should be considered comprehensively. Certainly, with the consideration of the self-powered/low-powered operation, the application of weak light (low light intensity) means the less dependence on light or less energy needed, that is, illumination with 940 nm is the best choice.

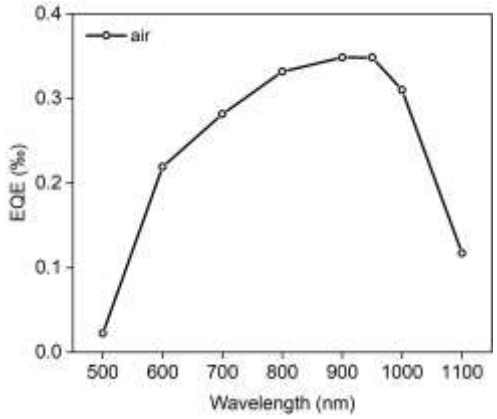

Fig. 8. External quantum efficiency (EQE) spectrum of the N-Si sensor with the lateral structure.

4. Conclusion

In this work, the NO_2 sensing performance of a novel self-powered sensor based on the N-Si material and irradiated with the asymmetric light illumination is investigated at different light intensity and wavelength. With the increase of light intensity, the gas response has a maximum value at a certain optimal power density, which is caused by the competition between the baseline photocurrent and the NO_2-induced photocurrent change. Interestingly, there is also a shortest response time appearing at the same optimal power density. As to the sensitivity and the detectable range, however, they increase monotonously with the light intensity. At different wavelengths, the dependence of sensing parameters on light intensity present similar trends but the specific characteristic values are different, e.g., the optimal power density, the maximum gas response and the shortest response time. That is, besides the light intensity, the wavelength is another dimension to regulate/optimize the sensing characteristics. The multi-dimensional regulation of gas sensing provides more potential and possibility to effectively adjust/optimize the sensing properties. The choice of NIR wavelength 940 nm

with intensity of ~18 μW/cm^2 is a good example, at which the sensor simultaneously possesses low power consumption (low light power needed), good gas response, high sensitivity, wide detectable range, and short response time at room temperature. This excellent comprehensive performance at 940 nm is related to the highest EQE of the material appearing at around 950 nm.

CRediT author statement:

Yang Zhao: Conceptualization, Methodology, Investigation, Visualization, Writing - Original Draft. **Xiao-Long Liu:** Conceptualization, Writing - Review & Editing. **Sheng-Xiang Ma:** Conceptualization, Investigation. **Wen-Jing Wang:** Investigation. **Xi-Jing Ning:** Supervision. **Li Zhao:** Supervision. **Jun Zhuang:** Validation, Writing - Review & Editing, Supervision.

Declaration of interests

The authors declare that they have no known competing financial interests or personal relationships that could have appeared to influence the work reported in this paper.

Acknowledgements

This work is supported by the National Natural Science Foundation of China under grant no. 6207030573, the National Basic Research Program of China (973 Program) under grant no. 2012CB934200, and the Specialized Research Fund for the Doctoral Program of Higher Education under grant no. 20130071110018.

Appendix A. Supplementary material

Supplementary material associated with this article is available. Light intensity improved low concentration detectable limit, light intensity regulated gas sensing properties under illumination of 455 nm and 940 nm and effects of relative humidity (RH) on gas sensing properties.

References

[1] T.L. Shen, Y.W. Chu, Y.K. Liao, W.Y. Lee, H.C. Kuo, T.Y. Lin, Y.F. Chen, Ultrahigh-performance self-powered flexible photodetector driven from photogating, piezo-phototronic, and ferroelectric effects, Adv. Opt. Mater. 8 (2020) 1–8. https://doi.org/10.1002/adom.201901334.

[2] X. Li, C. Luo, H. Ji, Y. Zhuang, H. Zhang, V.C.M. Leung, Energy consumption optimization for self-powered IoT networks with non-orthogonal multiple access, Int. J. Commun. Syst. 33 (2020) 1–15. https://doi.org/10.1002/dac.4174.

[3] M. Shirvanimoghaddam, K. Shirvanimoghaddam, M.M. Abolhasani, M. Farhangi, V. Zahiri Barsari, H. Liu, M. Dohler, M. Naebe, Towards a green and self-powered internet of things using piezoelectric energy harvesting, IEEE Access. 7 (2019) 94533–94556. https://doi.org/10.1109/ACCESS.2019.2928523.

[4] J. Wang, T. He, C. Lee, Development of neural interfaces and energy harvesters towards self-powered implantable systems for healthcare monitoring and rehabilitation purposes, Nano Energy. 65 (2019) 104039. https://doi.org/10.1016/j.nanoen.2019.104039.

[5] P.N. Manikandan, H. Imran, V. Dharuman, Self-powered polymer-metal oxide hybrid solar cell for non-enzymatic potentiometric sensing of bilirubin, Med. Devices Sensors. 2 (2019). https://doi.org/10.1002/mds3.10031.

[6] R.L. Arechederra, S.D. Minteer, Self-powered sensors, Anal. Bioanal. Chem. 400 (2011) 1605–1611. https://doi.org/10.1007/s00216-011-4782-0.

[7] Z.L. Wang, On Maxwell's displacement current for energy and sensors : the origin of nanogenerators, Materials Today 20 (2017) 74-82. https://doi.org/10.1016/j.mattod.2016.12.001.

[8] P. Glynne-Jones, N.M. White, Self-powered systems: a review of energy sources, Sens. Rev. 21 (2001) 91–98.

[9] Y. Vashpanov, J. Il Jung, K. dal Kwack, Photo-EMF sensitivity of porous silicon thin layer-crystalline silicon heterojunction to ammonia adsorption, Sensors. 11 (2011) 1321–1327. https://doi.org/10.3390/s110201321.

[10] M.W.G. Hoffmann, A.E. Gad, J.D. Prades, F. Hernandez-Ramirez, R. Fiz, H. Shen, S. Mathur, Solar diode sensor: Sensing mechanism and applications, Nano Energy. 2 (2013) 514–522. https://doi.org/10.1016/j.nanoen.2012.12.003.

[11] M.W.G. Hoffmann, L. Mayrhofer Dr, O. Casals Dr, L. Caccamo, F. Hernez-Ramirez, G. Lilienkamp, W. Daum, M. Moseler, A. Waag, H. Shen, J.D. Prades, A highly selective and self-powered gas sensor via organic surface functionalization of p-Si/n-ZnO diodes, Adv. Mater. 26 (2014) 8017–8022. https://doi.org/10.1002/adma.201403073.

[12] A. Gad, M.W.G. Hoffmann, O. Casals, L. Mayrhofer, C. Fàbrega, L. Caccamo, F. Hernández-Ramírez, M.S. Mohajerani, M. Moseler, H. Shen, A. Waag, J.D. Prades, Integrated strategy toward self-powering and selectivity tuning of semiconductor gas sensors, ACS Sensors. 1 (2016) 1256–1264. https://doi.org/10.1021/acssensors.6b00508.

[13] Y. Jia, Z. Zhang, L. Xiao, R. Lv, Carbon nanotube-silicon nanowire heterojunction solar cells with gas-dependent photovoltaic performances and their application in self-powered NO_2 detecting, Nanoscale Res. Lett. 11 (2016) 0–5. https://doi.org/10.1186/s11671-016-1514-6.

[14] X. Hu, P. Hou, C. Liu, H. Cheng, Carbon nanotube/silicon heterojunctions for photovoltaic applications, Nano Mater. Sci. 1 (2019) 156–172. https://doi.org/10.1016/j.nanoms.2019.03.001.

[15] D. Liu, Q. Chen, A. Chen, J. Wu, Self-powered gas sensor based on SiNWs/ITO photodiode, RSC Adv. 9 (2019) 23554–23559. https://doi.org/10.1039/c9ra02972a.

[16] X.L. Liu, Y. Zhao, W.J. Wang, S.X. Ma, X.J. Ning, L. Zhao, J. Zhuang, Photovoltaic self-powered gas sensing: A review, IEEE Sensors Journal, https://doi.org/10.1109/JSEN.2020.3037463.

[17] X.L. Liu, Y. Zhao, S.X. Ma, S.W. Zhu, X.J. Ning, L. Zhao, J. Zhuang, Rapid and wide-range detection of NO_x gas by N-hyperdoped silicon with the assistance of a photovoltaic self-powered sensing mode, ACS Sensors. 4 (2019) 3056–3065. https://doi.org/10.1021/acssensors.9b01704.

[18] X.L. Liu, S.W. Zhu, H. Bin Sun, Y. Hu, S.X. Ma, X.J. Ning, L. Zhao, J. Zhuang, “Infinite sensitivity” of black silicon ammonia sensor achieved by optical and electric dual drives, ACS Appl. Mater. Interfaces. 10 (2018) 5061–5071. https://doi.org/10.1021/acsami.7b16542.

[19] X.L. Liu, S.X. Ma, S.W. Zhu, Y. Zhao, X.J. Ning, L. Zhao, J. Zhuang, Light stimulated and regulated gas sensing ability for ammonia using sulfur-hyperdoped silicon, Sensors Actuators, B Chem. 291 (2019) 345–353. https://doi.org/10.1016/j.snb.2019.04.073.

[20] X.L. Liu, Y. Zhao, L. Zhao, J. Zhuang, Light-enhanced room-temperature gas sensing performance of femtosecond-laser structured silicon after natural aging, Opt. Express. 28 (2020) 7237. https://doi.org/10.1364/oe.377244.

[21] J.L. Hou, C.H. Wu, T.J. Hsueh, Self-biased ZnO nanowire humidity sensor vertically integrated on triple junction solar cell, Sensors Actuators, B Chem. 197 (2014) 137–141. https://doi.org/10.1016/j.snb.2014.02.073.

[22] Y.M. Juan, S.J. Chang, H.T. Hsueh, T.C. Chen, S.W. Huang, Y.H. Lee, T.J. Hsueh, C.L. Wu, Self-powered hybrid humidity sensor and dual-band UV photodetector fabricated on back-contact photovoltaic cell, Sensors Actuators, B Chem. 219 (2015) 43–49. https://doi.org/10.1016/j.snb.2015.05.020.

[23] R. Tanuma, M. Sugiyama, Polycrystalline SnO_2 Visible-light-transparent CO_2 sensor integrated with NiO/ZnO solar cell for self-powered devices, Phys. Status Solidi Appl. Mater. Sci. 216 (2019) 1–5. https://doi.org/10.1002/pssa.201800749.

[24] X. Dong, N. Li, Z. Zhu, H. Shao, X. Rong, C. Liang, H. Sun, G. Feng, L. Zhao, A nitrogen-hyperdoped silicon material formed by femtosecond laser irradiation, 091907 (2014). https://doi.org/10.1063/1.4868017.

[25] C. Wu, C.H. Crouch, L. Zhao, J.E. Carey, R. Younkin, J.A. Levinson, E. Mazur, R.M. Farrell, P. Gothoskar, A. Karger, Near-unity below-band-gap absorption by microstructured silicon, Appl. Phys. Lett. 78 (2001) 1850–1852. https://doi.org/10.1063/1.1358846.

[26] C.H. Crouch, J.E. Carey, M. Shen, E. Mazur, F.Y. Génin, Infrared absorption by sulfur-doped silicon formed by femtosecond laser irradiation, Appl. Phys. A Mater. Sci. Process. 79 (2004) 1635–1641. https://doi.org/10.1007/s00339-004-2676-0.

[27] J.E. Carey, C.H. Crouch, M. Shen, E. Mazur, Visible and near-infrared responsivity of femtosecond-laser microstructured silicon photodiodes, Opt. Lett. 30 (2005) 1773. https://doi.org/10.1364/ol.30.001773.

[28] S.X. Ma, X.L. Liu, H.B. Sun, Y. Zhao, Y. Hu, X.J. Ning, L. Zhao, J. Zhuang, Enhanced responsivity of co-hyperdoped silicon photodetectors fabricated by femtosecond laser irradiation in a mixed SF_6 /NF_3 atmosphere, J. Opt. Soc. Am. B. 37 (2020) 730. https://doi.org/10.1364/josab.374044.

[29] B.P.J. de Lacy Costello, R.J. Ewen, N.M. Ratcliffe, M. Richards, Highly sensitive room temperature sensors based on the UV-LED activation of zinc oxide nanoparticles, Sensors Actuators, B Chem. 134 (2008) 945–952. https://doi.org/10.1016/j.snb.2008.06.055.

[30] Z. Yang, L. Guo, B. Zu, Y. Guo, T. Xu, X. Dou, CdS/ZnO core/shell nanowire-built films for enhanced photodetecting and optoelectronic gas-sensing applications, Adv. Opt. Mater. 2 (2014) 738–745. https://doi.org/10.1002/adom.201400086.

[31] H. Chen, M. Zhang, B. Xing, X. Fu, R. Bo, H.K. Mulmudi, S. Huang, A.W.Y. Ho-Baillie, K.R. Catchpole, A. Tricoli, Superior self-charged and -powered chemical sensing with high performance for NO_2 detection at room temperature, Adv. Opt. Mater. 8 (2020) 1–8. https://doi.org/10.1002/adom.201901863.

[32] D.W. Boeringer, R. Tsu, Lateral photovoltaic effect in porous silicon, Appl. Phys. Lett. 65 (1994) 2332–2334. https://doi.org/10.1063/1.112733.

[33] A. Srivastava, S.C. Agarwal, Lateral photovoltage in hydrogenated amorphous silicon, J. Non. Cryst. Solids. 227–230 (1998) 259–262. https://doi.org/10.1016/S0022-3093(98)00064-7.

[34] C.Q. Yu, H. Wang, Large near-infrared lateral photovoltaic effect observed in Co/Si metal-semiconductor structures, Appl. Phys. Lett. 96 (2010) 1–4. https://doi.org/10.1063/1.3419903.

Author biographies and photographs

Yang Zhao received her B.S. degree from China University of Petroleum, Qingdao, in 2018. She is studying for her master degree at Fudan University, Shanghai, in 2020, under the guidance of Prof. Jun Zhuang and Prof. Li Zhao. Her research is currently focused on fs-laser fabricated black silicon for gas sensors and photodetectors.

Jun Zhuang is a professor in the Department of Optical Science and Engineering, Fudan University, Shanghai. He completed his Ph.D. at the Shanghai Institute of Optics and Fine Mechanics in 1996. His research interests are the properties of functional materials, and their applications in optoelectronics, photovoltaics, and gas sensing, etc.